BIOCHEMISTRY
including biophysical chemistry & molecular biology
Article

Biochemistry **2010,** *49,* 1689–1701 1689
DOI: 10.1021/bi901970c

Biophysical and X-ray Crystallographic Analysis of Mps1 Kinase Inhibitor Complexes[†,‡]

Matthew L. H. Chu,[§,+,▽] Zhaolei Lang,[§,▽] Leonard M. G. Chavas,[∥] João Neres,[§] Olga S. Fedorova,[⊥] Lydia Tabernero,[#] Mike Cherry,[○] David H. Williams,[△] Kenneth T. Douglas,[§] and Patrick A. Eyers*[,◇]

[§]*Wolfson Centre for Structure-Based Rational Design of Molecular Diagnostics, School of Pharmacy and Pharmaceutical Sciences, University of Manchester, Manchester M13 9PL, U.K.,* [∥]*Structural Biology Research Center, Photon Factory, Institute of Materials Structure Science, High Energy Accelerator Research Organization (KEK), Tsukuba, Japan,* [⊥]*Institute of Chemical Biology and Fundamental Medicine, Siberian Branch of the Russian Academy of Sciences, Novosibirsk 630090, Russia,* [#]*Faculty of Life Sciences, Michael Smith Building, University of Manchester, Manchester M13 9PT, U.K.,* [○]*Accelrys, Cambridge Science Park, Cambridge, Cambridge CB4 OWN, U.K.,* [△]*Summit PLC, Oxford OX14 4RY, U.K., and* [◇]*YCR Institute for Cancer Studies, University of Sheffield, Sheffield S10 2RX, U.K.* [+]*Current address: Department of Structural Biology, Stanford University School of Medicine, Stanford, CA 94305.* [▽]*These authors contributed equally to this work.*

Received November 15, 2009; Revised Manuscript Received January 25, 2010

ABSTRACT: The dual-specificity protein kinase monopolar spindle 1 (Mps1) is a central component of the mitotic spindle assembly checkpoint (SAC), a sensing mechanism that prevents anaphase until all chromosomes are bioriented on the metaphase plate. Partial depletion of Mps1 protein levels sensitizes transformed, but not untransformed, human cells to therapeutic doses of the anticancer agent Taxol, making it an attractive novel therapeutic cancer target. We have previously determined the X-ray structure of the catalytic domain of human Mps1 in complex with the anthrapyrazolone kinase inhibitor SP600125. In order to validate distinct inhibitors that target this enzyme and improve our understanding of nucleotide binding site architecture, we now report a biophysical and structural evaluation of the Mps1 catalytic domain in the presence of ATP and the aspecific model kinase inhibitor staurosporine. Collective *in silico*, enzymatic, and fluorescent screens also identified several new lead quinazoline Mps1 inhibitors, including a low-affinity compound termed Compound 4 (Cpd 4), whose interaction with the Mps1 kinase domain was further characterized by X-ray crystallography. A novel biophysical analysis demonstrated that the intrinsic fluorescence of SP600125 changed markedly upon Mps1 binding, allowing spectrophotometric displacement analysis and determination of dissociation constants for ATP-competitive Mps1 inhibitors. By illuminating the structure of the Mps1 ATP-binding site our results provide novel biophysical insights into Mps1−ligand interactions that will be useful for the development of specific Mps1 inhibitors, including those employing a therapeutically validated quinazoline template.

Protein kinases represent important validated drug targets in human disease, and a dozen or so small molecule kinase inhibitors have now been approved for clinical use (*1*, *2*). In order to maintain this momentum and develop inhibitors of new oncology targets, including protein kinases that control progression through mitosis, several obstacles must first be overcome. These include high-resolution structural analysis of target kinases and the synthesis and structural validation of drug-like small molecule kinase inhibitors. One valuable approach for achieving these goals is through the application of fragment-based screening methodologies, in which biochemically validated drug-like inhibitor scaffolds are cocrystallized with appropriate kinases prior to iterative rounds of chemical modification and structure determination (*3*, *4*).

The human dual specificity kinase Mps1,[1] also termed TTK, has emerged as a master mitotic enzyme, with roles in chromosome alignment and as a regulator of the spindle assembly checkpoint (SAC), which operates in eukaryotes to help to prevent the emergence of aneuploidy (*5*, *6*). Mps1 enzymatic activity is controlled by reversible autophosphorylation of conserved residues in the activation segment, which has been examined experimentally through biochemical, cellular, and structural approaches (*7*−*12*). The mechanism of autoactivation is likely to involve phosphorylation-dependent stabilization of the active, closed configuration, although in the absence of an appropriately phosphorylated Mps1 catalytic domain structure, it is not yet clear how this compares in three-dimensional terms with that of the dephosphorylated inactive kinase (*11*, *12*). The central role of Mps1 in mitotic mechanisms has raised the possibility that this kinase might represent an attractive novel therapeutic anticancer target for small molecule inhibitor discovery (*13*). Mps1 mRNA overexpression has been reported in several tumor types (*14*), and the potential advantages of inhibiting Mps1 in combination with therapeutic doses of Taxol have recently been highlighted in human cancer cells using RNAi approaches (*15*). On the other hand, the finding that Mps1 ablation induces experimental resistance to high concentrations

[†]We are grateful to the Faculty of Medical and Human Sciences, University of Manchester, for overseas research scholarships (to M.L. H.C. and Z.L.), the Portuguese Foundation for Science and Technology for support (to J.N.), and the U.K. Medical Research Council for a Career Development Fellowship (to P.A.E.).

[‡]The coordinates for the Mps1 complexes have been deposited in the PDB with accession numbers 3HMN (Mps1−ATP), 3HMO (Mps1−staurosporine), and 3HMP (Mps1−Compound 4).

*To whom correspondence should be addressed. Phone: +44 114 226 1295. Fax: +44 114 271 3515. E-mail: p.eyers@sheffield.ac.uk.

Published on Web 01/25/2010

of Taxol (*16*) makes the discovery and assessment of Mps1 inhibitors a high priority in the context of cancer chemotherapy.

In the past few years, several experimental Mps1 inhibitors have been described, including the low-affinity compound cincreasin, which inhibits the budding yeast Mps1 homologue with low potency but high specificity (*17*), and the nonspecific anthrapyrazolone inhibitor SP600125 (*18*), which directly inhibits Mps1 activity *in vitro* and induces some effects consistent with Mps1 inhibition in cells (*11*, *19*). The promiscuous bisindolylmaleimide kinase inhibitor staurosporine has also been reported to interact with the Mps1 ATP-binding site (*20*), although its high affinity for nearly all protein kinases and consequential cellular toxicity prevent its further exploitation for investigation of Mps1 biology. This compound has instead become a useful analytical tool for comparing the inhibitor interface of different kinase catalytic domains, given the enormous range of affinities that it exhibits toward members of the human kinome (*20*).

In this paper, we have investigated a diverse panel of Mps1 inhibitors using combined *in silico*, radiometric, fluorescent, and crystallographic approaches. We demonstrate that the fluorescence emission spectrum of SP600125 becomes altered substantially upon kinase binding, allowing us to exploit this molecule as a novel probe for Mps1 ATP-binding site occupancy. This provides a simple new means to study the nucleotide-binding pocket of both active and inactive Mps1 and permits quantitative extraction of binding data for ATP-competitive Mps1 inhibitors. To stimulate the discovery of such molecules, we also report the structure of the dephosphorylated Mps1 catalytic domain in the presence of ATP, staurosporine, and a novel quinazoline ligand. Our findings will be valuable for further Mps1 small molecule inhibitor discovery and validation.

EXPERIMENTAL PROCEDURES

Compound Library Selection and Identification of Mps1 Inhibitors. We initially screened for Mps1 inhibitors using a compound library containing a broad selection of representative kinase inhibitor scaffolds selected from a 160-member compound library. The library was kindly supplied by Sareum PLC, and compounds had previously been chosen from chemical vendor catalogues by *in silico* screening of protein kinase ATP-binding sites (*21*). Specifically, compound collections from commercial vendors (including Asinex, ChemDiv, Examine, IBS, Maybridge, and SPECs) were initially filtered using the software package Pipeline Pilot (Accelrys) to provide approximately 15000 scaffold-like molecules for *in silico* screening. A protocol was written in Pipeline Pilot, which consisted of a series of filters that systematically reduced the vendor compounds to a unique set of template-like molecules. The protocol first standardized vendor compounds by removing additional components, such as salts, and by transforming each molecule to the canonical tautomer. Two customized filters were then applied. The first filter was used in the protocol to remove undesirable, potentially toxic or chemically reactive groups that might be detrimental to biological systems (Supporting Information Table S1). Next, a "drug-like" filter was applied prior to the second customized template-like filter, which defined the desirable compound scaffold properties (Supporting Information Table S2). The remaining compounds were then duplicate-checked, and a single file was created for use in a 3-D screen.

Our initial inhibitor scaffold screening set was used in a 3-D pharmacophore search using the software package MOE (Chemical Computing Group) with an *in silico* hit being defined as a compound that matched at least three of five desirable features of known kinase inhibitors (Figure 1A) and which fell within a set volume constraint. To set up the volume constraint, exclusion volume spheres of 2 Å were applied to the nonhydrogen protein atoms surrounding the ATP-binding site of the cAMP-dependent protein kinase (PKA; PDB accession code 1ATP). These were then combined, and a hit was rejected if any of its atoms fell inside this combined exclusion volume. The pharmacophore query was built by overlaying the active ATP-binding sites of several protein kinase structures to define the specific pharmacophore points within a protein kinase active site. The library was selected as a kinase-biased scaffold set from which a subset could be readily interrogated for any kinase-specific screen, so structures were chosen across a range of protein kinase subfamilies based on their conformation, the structural resolution, and completeness around the active site. Structures included representatives of PKA, Chk1, p38, CDK2, and Aurora A (respective PDB codes: 1ATP, 1IA8, 1FIN, 1OUY, and 1OL7). Compounds identified from the *in silico* search were separated into different chemotype clusters based on the core rings from each compound and then manually assessed prior to selection of specific compounds for Mps1 library inclusion. The average physicochemical properties of the compound library were as follows: molecular mass 250 Da, ALogP value 2.0, H-bond acceptor count 3.0, H-bond donor count 1.5, and three rotatable covalent bonds.

SP600125 and staurosporine (Figure 1B) were purchased from Calbiochem and stored in DMSO at 10 mM at −20 °C. Six low-affinity Mps1 inhibitors, termed Compounds (Cpds) 1−6 (Figure 1B), were identified biochemically from the 160-member compound library, using a radiometric *in vitro* enzyme assay with Sf9-expressed full-length human Mps1 and the exogenous substrate myelin basic protein (MBP) as substrate in the presence of 100 μM ATP (*9*). Test compounds (stored in DMSO at 10 mM at −20 °C) were screened in duplicate at a concentration of 50 μM, and the low background signal of the *in vitro* assay was sufficient to allow scaffold inhibitors with relatively low IC_{50} values toward human Mps1 to be rapidly identified. Initial hits, defined as compounds inhibiting Mps1 (but not Aurora A) activity by ≥20% at a concentration of 50 μM, were validated by duplicate screening using the bacterially expressed human Mps1 catalytic domain. For titrations, 500 ng of the purified active Mps1 catalytic domain (residues 510−809) was mock-incubated or incubated with inhibitors at the appropriate concentration for 5 min at room temperature and assayed with 20 μg of MBP for 30 min at 30 °C, in the presence of 100 μM [γ-^{32}P]ATP (specific activity 500 cpm/pmol) as described previously (*9*, *11*).

Cloning, Expression, Purification, and Crystallization of Mps1 Catalytic Domain. cDNA encoding amino acid residues 510−809 of human Mps1 (including the complete catalytic domain encompassing residues 525−791) was amplified by PCR and cloned into the vector pET-30 Ek/LIC (Novagen). The recombinant His-tagged proteins were expressed, purified, and dephosphorylated as described previously for Mps1 (residues 510−857), whose crystal structure we have previously reported (*11*). Mps1 (10 mg/mL, dephosphorylated with lambda (λ) phosphatase) was crystallized using vapor-diffusion methods in a reservoir solution containing 0.1 M HEPES (pH 6.0), 12.5% (w/v) polyethylene glycol (PEG) 300, 5% (w/v) glycerol, 2.5% (w/v) 2-propanol, and 50 mM ammonium sulfate at 20 °C. The apo-Mps1 crystals were soaked in reservoir solution containing 25 mM ATP (disodium salt hydrate, Sigma), 0.5 mM

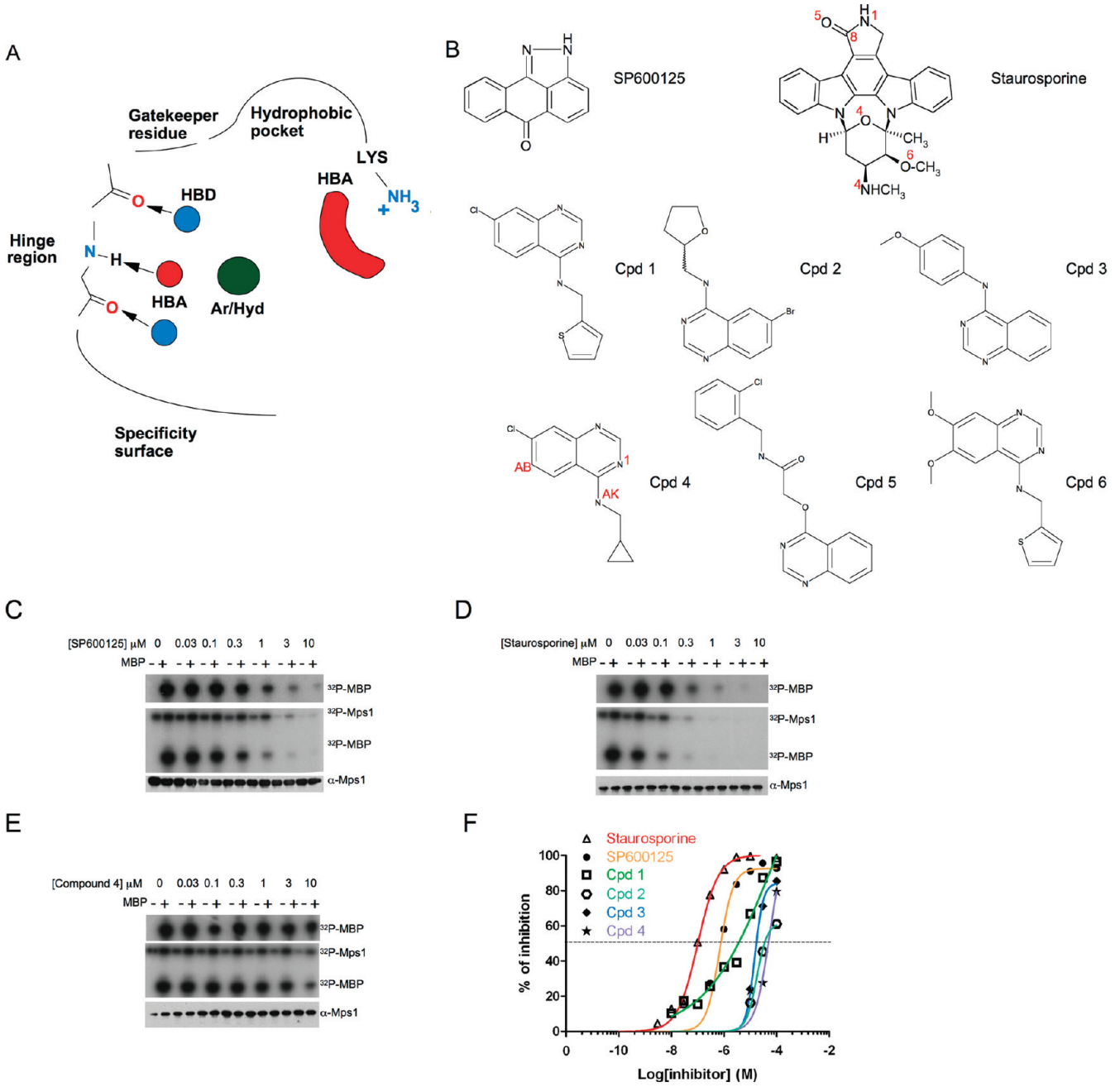

FIGURE 1: Biochemical assays for analysis of Mps1 inhibitors. (A) Schematic of the 3-D pharmacophore search performed using the molecular operating environment (MOE). In addition to the features shown, volume constraints were applied to limit the scope of the hits identified, and the donor/acceptor features for the kinase hinge region were directional. Key: HBD, hydrogen bond donor; HBA, hydrogen bond acceptor; Ar/Hyd, aromatic or hydrophobic group; LYS, lysine. (B) Chemical structure and suggested numbering of Mps1 inhibitors. (C−E) Kinase assay of the recombinant His-tagged Mps1 catalytic domain (top panels) or λ phosphatase-treated Mps1 (middle panels) in the presence of the indicated concentration of inhibitor and the presence or absence of the exogenous Mps1 substrate MBP. Equal Mps1 loading was confirmed by immunoblotting with a polyclonal Mps1 antibody (bottom panels). Note the phosphorylation of both MBP and Mps1 in λ phosphatase-treated panels and their dual sensitivity to inhibition by each compound. (F) Titration curves for inhibition of the Mps1 catalytic domain. Active (phosphorylated) Mps1 proteins were titrated in triplicate with SP600125 (orange), staurosporine (red), Cpd 1 (green), Cpd 2 (cyan), Cpd 3 (blue), or Cpd 4 (purple) at 0.0001, 0.0003, 0.001, 0.003, 0.01, 0.03, 0.1, 0.3, 1, 3, 10, 30, and 100 μM. After SDS−PAGE, ^{32}P incorporation into the exogenous substrate MBP was determined by Cerenkov counting in a scintillation counter. The best-fit titration curves were plotted based on the "log(inhibitor) vs response" model $Y = \text{bottom} + (\text{top} - \text{bottom})/[1 + 10^{(X-\log IC_{50})}]$ using GraphPad Prism software, and calculated IC_{50} values are presented for each compound. Similar results were seen in at least two independent experiments.

staurosporine ((9*S*,10*R*,11*R*,13*R*)-2,3,10,11,12,13-hexahydro-10-methoxy-9-methyl-11-(methylamino)-9,13-epoxy-1*H*,9*H*-diindolo-[1,2,3-*gh*:3′,2′,1′-*lm*]pyrrolo[3,4-*j*][1,7]benzodiazonin-1-one), or 0.5 mM Cpd 4 (7-chloro-*N*-(cyclopropylmethyl)quinazolin-4-amine) for 5 min prior to cryoprotection.

Data Collection, Structure Determination, and Refinement. Prior to data collection, ATP or inhibitor-soaked crystals were transferred to a cryoprotectant solution consisting of reservoir solution and 25% (v/v) PEG 300 for 1 min and then flash-frozen under a nitrogen stream. X-ray diffraction data of Mps1−ATP were collected on a Raxis IV++ image-plate detector at a wavelength of 1.54 Å using an in-house rotating anode Rigaku MicroMax007 X-ray generator. Data for Mps1−staurosporine and Mps1−Cpd 4 were collected on

beamline I03 at a wavelength of 0.92 Å (Diamond Light Source, Didcot, U.K.). All diffraction data were integrated and scaled using iMosflm (*22*) and Scala (*23*), respectively, and all of the Mps1−ligand complex structures were solved by molecular replacement using the coordinates of Mps1 extracted from the structure of the Mps1−SP600125 complex (PDB 2ZMD, ref *11*). Crystallographic refinement and model fitting were performed using Refmac5 (*24*), Phenix (*25*), and Coot (*26*). The data-processing and refinement statistics are summarized in Table 2. X-ray diffraction data of each data set were indexed in the space group *I*222 with the following unit cell parameters: a = 70.98 Å, b = 104.95 Å, c = 111.02 Å (Mps1−ATP), a = 70.94 Å, b = 103.88 Å, c = 111.42 Å (Mps1−staurosporine), and a = 71.37 Å, b = 103.93 Å, c = 111.73 Å (Mps1−Cpd 4) crystals. The stereochemistry of the final models was assessed using MolProbity (*27*). All structural figures were prepared with PyMOL (*28*). Atomic coordinates and structure factors have been deposited in the PDB under the following accession ID's: 3HMN (Mps1−ATP), 3HMO (Mps1−staurosporine), and 3HMP (Mps1−Cpd 4).

Fluorescence Measurements. Fluorescence emission spectra were recorded on a Varian Eclipse fluorescence spectrophotometer with a Peltier-thermostated cuvette holder. Spectra were recorded in 100 μL volume thermostated, four-sided, quartz cuvettes at 25 °C and corrected for buffer emission and volume changes. Spectra of systems containing Mps1 were recorded in 50 mM Tris-HCl (pH 7.4) buffer containing 150 mM NaCl and 0.1 mM EGTA. Excitation wavelengths for most assays were 404 nm. In most cases slit widths were set from 5 to 10 nm for emission spectra, depending on the intensity of emission. An "automatic shutter-on" regime was applied to minimize photodegradation of compounds in the cuvettes.

UV Spectroscopy. UV−visible absorption spectra were measured at 25 °C on a Cary-Varian 4000 UV−visible spectrophotometer with a Peltier-thermostated cuvette holder. Spectra were recorded in 2 mL volume thermostated, four-sided, quartz cuvettes.

Methods for Calculating K_d Values. The fluorescence intensity of SP600125 ([SP]) at the emission maximum (508 nm) was used to calculate the dissociation constant K_d, corresponding to the interaction with enzyme ([E]):

$$\mathrm{SP} + \mathrm{E} \leftrightarrows \mathrm{E}\cdot\mathrm{SP} \quad (1)$$

$$K_d = \frac{[\mathrm{SP}][\mathrm{E}]}{[\mathrm{E}\cdot\mathrm{SP}]} \quad (2)$$

The intensity of detected fluorescence F is expressed as

$$F = f_{SP}[\mathrm{SP}] + f_{ESP}[\mathrm{E}\cdot\mathrm{SP}] \quad (3)$$

where f_{SP} and f_{ESP} are the partial fluorescence intensities of free and complexed SP600125, respectively. The values of K_d, f_{SP}, and f_{ESP} were fitted by a nonlinear regression procedure using SigmaPlot 9.0 software (Jandel Scientific). When ATP or staurosporine was added to the mixture of SP600125 with Mps1 enzyme, the fluorescence intensities of SP600125 were corrected for quenching effects using the Stern−Volmer equation. The reversible formation of complexes of these molecules with enzyme were taken into account:

$$\mathrm{ATP} + \mathrm{E} \leftrightarrows \mathrm{ATP}\cdot\mathrm{E} \quad (4)$$

$$\text{staurosporine} + \mathrm{E} \leftrightarrows \text{staurosporine}\cdot\mathrm{E} \quad (5)$$

The exact mathematical expression describing two-ligand competitive binding of SP600125 and ATP or staurosporine to Mps1 was used to calculate the concentrations of [SP] and [E·SP] according to ref *29*.

RESULTS

Biochemical Assays for Analysis of Mps1 Inhibitors. We initially investigated the *in vitro* effects of a panel of Mps1 inhibitors, including the commercially available nonspecific compounds SP600125 and staurosporine, and a series of quinazoline compounds (Figure 1B), which as a chemical class are valuable inhibitors of numerous protein kinases, including Aurora A and B (*30*, *31*). Six promising quinazoline compounds were identified from a chemical fragment-type screen, in which a library of *in silico*-selected compounds with desirable kinase inhibitory properties (Figure 1A) was screened at a fixed concentration of 50 μM for inhibition of full- length His-tagged Mps1. Only those compounds that exhibited ≥20% Mps1 inhibition at 50 μM, with no inhibition of Aurora A, were selected for further investigation (data not shown). To assess inhibition in our standard radiometric Mps1 assay, which employs a bacterially expressed catalytic domain, we determined Mps1 kinase activity in the presence of increasing concentrations of each inhibitor (or DMSO as a solvent control) and a final ATP concentration of 100 μM, using the substrates MBP and Mps1 as described (*9*, *11*). Mps1 is phosphorylated and catalytically active when isolated from bacteria (*9*, *11*) and phosphorylates MBP (Figure 1C−E, top panels). High levels of Mps1 autophosphorylation during bacterial synthesis prevent these preparations from further autophosphorylation *in vitro*. In contrast, λ phosphatase-treated Mps1 (λ-Mps1), which crystallizes in an inactive conformation (*11*), becomes catalytically active after MgATP addition (*8*, *11*) when it phosphorylates MBP and also autophosphorylates itself efficiently (Figure 1C−E, middle panels), the latter event occurring through Mps1 trans-autophosphorylation (*7*, *8*). Mps1 Western blots demonstrate that equal amounts of kinase are present in SP600125, staurosporine, and Cpd 4 titrations (Figure 1C−E, bottom panels). The best-fit IC_{50} titration curves for Mps1 catalytic domain inhibition toward MBP are presented in Figure 1F for each individual compound. Inspection of the experimental autoradiographs shown in Figure 1C−E demonstrates dual inhibition of both MBP and Mps1 phosphorylation by SP600125, staurosporine, and Cpd 4. Among the eight compounds evaluated in this study, the known aspecific kinase inhibitors staurosporine and SP600125 exhibit the highest Mps1 inhibitory activity, with IC_{50} values of 0.102 ± 0.015 and 0.692 ± 0.12 μM, respectively, for MBP phosphorylation (Table 1). In contrast, the scaffold-like inhibitors Cpds 1−4 exhibit modest inhibition of Mps1, demonstrating a range of low to midmicromolar IC_{50} values, while Cpds 5 and 6 exhibit less than 50% inhibition, even at the highest tested concentration of 100 μM.

Validation of Mps1 Inhibitor Interaction Using a Novel Fluorescent Kinase Assay. One of the problems with comparing IC_{50} values for protein kinase inhibition by ATP-competitive inhibitors is that they vary as a function of ATP concentration, and this can differ markedly between studies depending upon assay design. Moreover, cellular ATP concentrations are in the low millimolar range, meaning that comparisons between experimental *in vitro* and cellular IC_{50} values are potentially futile. To help to overcome these issues, the intrinsic fluorescence of pan-kinase inhibitors, such as staurosporine, has recently been

Table 1: IC_{50} and K_d Values for Selected Mps1 Inhibitors[a]

compound	IC_{50} (μM)	$K_{d,app}$ (μM)	K_d (μM)[c]
staurosporine	0.102 ± 0.015	ND[b]	0.0305 ± 0.001
SP600125	0.692 ± 0.12	0.52 ± 0.02[c]/0.60 ± 0.06[d]	0.22 ± 0.02
Cpd 1	6.43 ± 0.65	26.4 ± 2.5	ND
Cpd 2	12.08 ± 2.3	ND	ND
Cpd 3	12.34 ± 2.4	ND	ND
Cpd 4	38.41 ± 4.6	13.2 ± 1.3	3.24 ± 0.28
Cpd 5	> 100	ND	ND
Cpd 6	> 100	312 ± 45	ND

[a]Mps1 inhibitor IC_{50} values were calculated from best-fit IC_{50} titration curves obtained through radiometric kinase assays using GraphPad Prism software. $K_{d,app}$ values were calculated from simple fluorescence displacement curves using the Mps1 catalytic domain or the λ phosphatase-treated Mps1 catalytic domain where indicated. K_d values were calculated for the binding of two different ligands competing for the same binding site on a protein using the mathematical expressions described in ref *29*. [b]Not determined. [c]Mps1 catalytic domain. [d]λ phosphatase-treated Mps1 catalytic domain.

exploited as a general probe for the calculation of inhibitor affinities toward kinases using the principle of competitive displacement (*32*−*34*). To investigate whether the experimental anthrapyrazolone SP600125 might also exhibit fluorescence in regions that are distinct from those usually exploited for investigating protein function, such as peptide bond and tryptophan emissions at 256 and 280 nm, we subjected it to biophysical scrutiny. As detailed in Figure 2A, the Mps1 inhibitor SP600125 is indeed a fluorescent molecule, with maximum fluorescence detected at 508 nm in Tris-HCl buffered medium at pH 7.4 (λ_{exc} 404 nm). Interestingly, by assessing fluorescence in a series of standard buffer solutions, we noted a close relationship between the increase in the maximum frequency of fluorescence emission and the polarity of the solvent (Figure 2B, inset). Moreover, a linear relation exists between SP600125 emission frequency and both the dielectric constant and the polarity parameter, E_T, of the solvent (Figure 2B, inset), suggesting that the relative fluorescence spectrum of SP600125 might be a useful surrogate reporter of the environment experienced upon binding to a hydrophobic pocket, such as the ATP-binding site of protein kinases. To test this hypothesis further, we next investigated the effects on SP600125 fluorescence spectra resulting from the addition of aliquots of the active, phosphorylated Mps1 catalytic domain to the inhibitor. As shown in Figure 3A, increasing the concentration of Mps1 led to a decrease in intensity of the band at 508 nm (labeled A) with λ_{em} moving gradually to lower wavelengths, culminating in a change in λ_{max} from 508 to 486 nm (labeled DEFG). The changes in intensity at 508 nm, corrected for volume changes arising during the addition of Mps1 aliquots (maximally 30%), were plotted as binding isotherms for a single-site binding equation of the form $FU = (FU)_{max}[protein]/(K_d + [protein])$. By the end of the titration the value of λ_{em} was 486 nm, and this led to a calculated dissociation constant (K_d) of 0.52 ± 0.02 μM for SP600125 and the active, phosphorylated Mps1 catalytic domain (Figure 3B). As a test of the reproducibility of this displacement assay, K_d was determined in three independent experiments, giving values of 0.51 ± 0.04, 0.54 ± 0.02, and 0.51 ± 0.02 μM, respectively. Similar data were obtained when dephosphorylated Mps1 was incubated in an identical fashion with SP600125 (Figure 3C), the calculated K_d value being 0.60 ± 0.06 μM (Figure 3D, n = 4 determinations). These novel fluorescent data clearly demonstrate that SP600125 can bind to both dephosphorylated and active (phosphorylated) Mps1 with

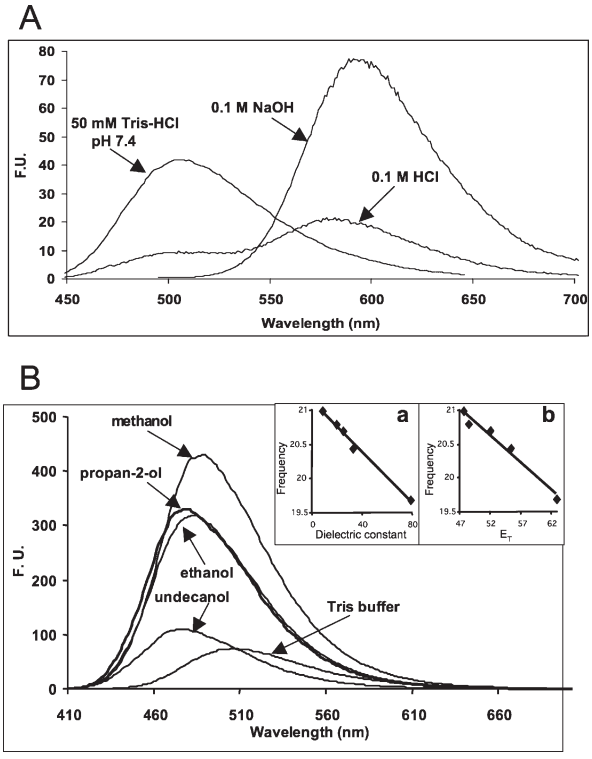

FIGURE 2: Analysis of SP600125 fluorescence. (A) Emission spectra at 25 °C of SP600125 (2 μM) in 0.1 M NaOH (λ_{exc} 484 nm) and 0.1 M HCl (λ_{exc} 404 nm) and at 50 nM final concentration in Tris buffer (50 mM Tris-HCl, pH 7.4, 150 mM NaCl, 0.1 mM EGTA, 1 mM DTT; λ_{exc} 404 nm). (B) Emission spectra at 25 °C of SP600125 (4 μM) in 50 mM Tris-HCl, pH 7.4, buffer and various organic solvents. The insets show plots of the frequency of maximum emission (10^3 cm^{-1}) versus (a) dielectric constants and (b) solvent polarity parameter (E_T) of various organic solvents. Points are experimental; lines are by least-squares linear regression analysis. The line in inset a had the equation (frequency) = 21.1 ± 0.04 − 0.0186 ± 0.001 (dielectric constant) (r^2 = 0.992); the line in inset b had the equation (frequency) = 24.8 ± 0.44 − 0.080 ± 0.008(E_T) (r^2 = 0.970).

similar affinity, in agreement with our biochemical assessment (Figure 1) and with structural analysis of SP600125 bound to a catalytically inactive Mps1 kinase domain mutant (*11*).

The low potency of the quinazoline Mps1 inhibitor series presented in Figure 1 was predictable due to the nature of the compounds, which were selected by *in silico* docking algorithms as ATP-binding site kinase inhibitor scaffolds. However, prior to embarking on structural studies, we wished to confirm whether these compounds directly interact with the nucleotide-binding site of Mps1, as has been previously demonstrated for both SP600125 and staurosporine (*11*, *19*, *20*). By utilizing our novel fluorescence-based SP600125 assay, we therefore investigated whether SP600125−Mps1 fluorescence was influenced by potential competing Mps1 ligands. As shown in Figure 4A,B, we found that incubation of the SP600125−Mps1 complex with increasing concentrations of MgATP led to a change in intensity of the band at 508 nm, with λ_{em} gradually shifting to higher wavelengths, suggesting displacement of SP600125 in a concentration-dependent manner by MgATP with a K_d of 0.22 μM. Interestingly, incubation with Cpd 4 or staurosporine also led to an increase in intensity of the band at 508 nm with λ_{em} gradually shifting to higher wavelengths, entirely consistent with competitive SP600125 displacement from the active site by both of these compounds (Figure 4C,E). The changes in intensity at 508 nm, corrected for volume changes arising during the addition, were

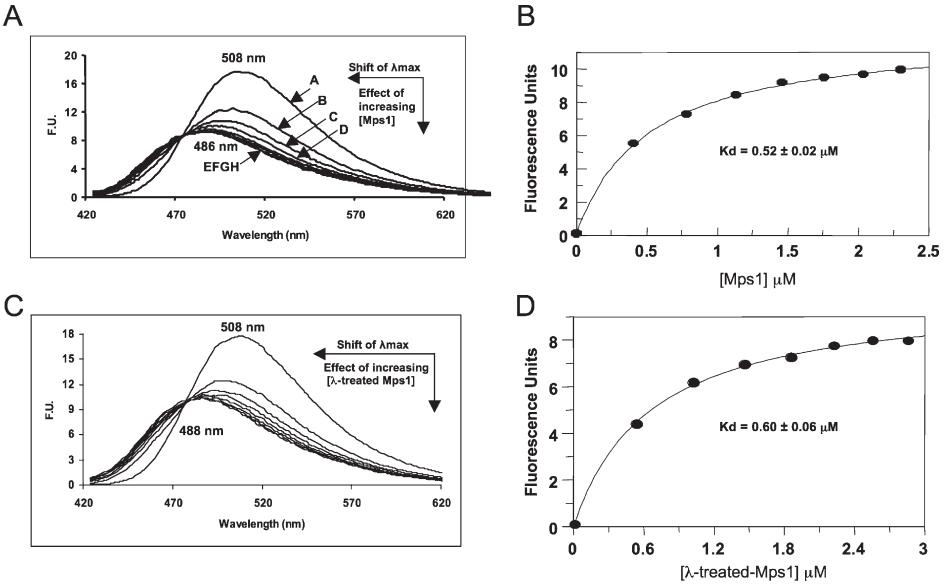

FIGURE 3: SP600125 fluorescence spectra measured upon Mps1 binding. (A) Fluorescence spectra resulting from stepwise addition of phosphorylated, active Mps1 to SP600125 (71.43 nM) in buffer (50 mM Tris-HCl, pH 7.4, 150 mM NaCl, 0.1 mM EGTA; λ_{exc} 404 nm). The spectra are annotated with the concentration of Mps1 (μM) present: A, 0; B, 0.411; C, 0.789; D, 1.139; E, 1.463; F, 1.765; G, 2.045; H, 2.308. (B) Binding curve for SP600125 titrated with increasing amounts of Mps1 plotting the change (decrease) in fluorescence intensity at 508 nm (FU) against the concentration of Mps1 after correction for volume changes during the titration. Points are experimental from the data in (A); the line is theoretical for single-site binding with K_d of 0.52 ± 0.02 μM and a limiting value of 12.17 ± 0.16 for FU. (C, D) As for (A) and (B), except λ phosphatase-treated (dephosphorylated) Mps1 (71.43 nM) was employed to calculate a theoretical single-site binding K_d value of 0.60 ± 0.06 μM.

then plotted as binding isotherms for a single-site binding equation producing an apparent dissociation constant of 13.2 ± 1.3 μM for Cpd 4 (Figure 4D). Simple competitive displacement binding curves of the form shown in Figure 3 were also obtained for Cpds 1 and 6, with K_d values of 26.4 ± 1.77 and 312 ± 32 μM, respectively (Table 1). However, Cpds 3 and 5 were intrinsically fluorescent, while Cpd 2 quenched the fluorescence of SP600125 in the concentration range 15−240 μM, limiting further analysis by this method. As depicted in Figure 4E, the incubation of the Mps1−SP600125 complex with staurosporine generated a more complex sigmoidal response, from which K_d values could not be extracted using a single-interaction site equation. To extract K_d values from these data, we employed a precise mathematical equation for two different ligands competing for the same binding site on a protein (*29*). Using this approach, we calculated a K_d of 0.0305 ± 0.001 μM for staurosporine and Mps1 binding (Table 1). Furthermore, by analyzing the tight binding of staurosporine to Mps1, we determined that some 50% of the recombinant Mps1 was competent to bind this inhibitor, presumably due to the presence of non-natively folded or denatured Mps1 in the preparation. This is in line with the known substoichiometric incorporation of phosphate into bacterially expressed human Mps1 (*35*) and its reduced specific activity when compared to human Mps1 overexpressed in eukaryotic Sf9 cells (*9*). However, recalculation of the K_d for Cpd 4 using a two-ligand equation and 52.8% of binding-competent enzyme gave a value of 3.24 ± 0.28 μM, similar to that calculated using the single-site method (Table 1). Taken together, the biophysical data presented in Figures 2−4 support the order of inhibitor potency derived from biochemically determined IC_{50} values (Figure 1). They are also entirely consistent with binding of all of these compounds to a hydrophobic environment in Mps1 and in complete agreement with our previous structural analysis of an Mps1 catalytic domain in complex with SP600125 (*11*).

Structural Analysis of ATP Binding to the Mps1 Catalytic Domain. To develop a structural understanding of Mps1 nucleotide binding, an important next step for aiding the rational design of potent and specific Mps1 inhibitors, we investigated the interaction of Mps1 with ATP, the physiological ligand (data set 3HMN, Table 2). The overall fold of the kinase domain of the Mps1−ATP complex (Figure 5A) is very similar to that of the Mps1−apo form, whose structure was originally determined using a recombinant Mps1 catalytic domain containing 48 additional residues at the C-terminus (*11*). Indeed, the C_α root-mean-square deviation (rmsd) is only 0.523 Å when 256 C_α atoms are aligned using the CCP4 program Superpose (*36*, *37*). Interestingly, our Mps1−ATP complex crystallizes in a conformation in which the nucleotide lies adjacent to a molecule of PEG from the experimental crystallization medium (Supporting Information Figure S1A), as previously described for both PEG-bound apo-Mps1 and a PEG and SP600125-complexed T686A Mps1 mutant (*11*). Consistent with structures of other reported kinases in complex with either ATP or nonhydrolyzable analogues (*38*−*42*), the adenine base of ATP binds near the hinge region of Mps1, forming a pair of conserved hydrogen bonds between N6 and the Glu-603 main-chain carbonyl oxygen and between N1 and the Gly-605 main-chain NH. Extensive van der Waals contacts are also made between the adenine base and Ile-531, Val-539, and Met-602 toward the N-terminal domain and Ile-586 and Leu-654 toward the C-terminal domain. The ribose of ATP does not interact directly with Mps1, although in other protein kinases hydrogen bonds often exist between the O2′-hydroxyl of the ribose and the carboxyl group of the residue at the equivalent position occupied by Asp-608 in Mps1 and from the O3′-hydroxyl to the main-chain carbonyl oxygen of the residue at the position equivalent to Ala-651 in Mps1. In our structure, the ribose group exhibits a clear electron density, probably because the adenine ring and the α-phosphate are stabilized so that conformational flexibility of the sugar moiety is

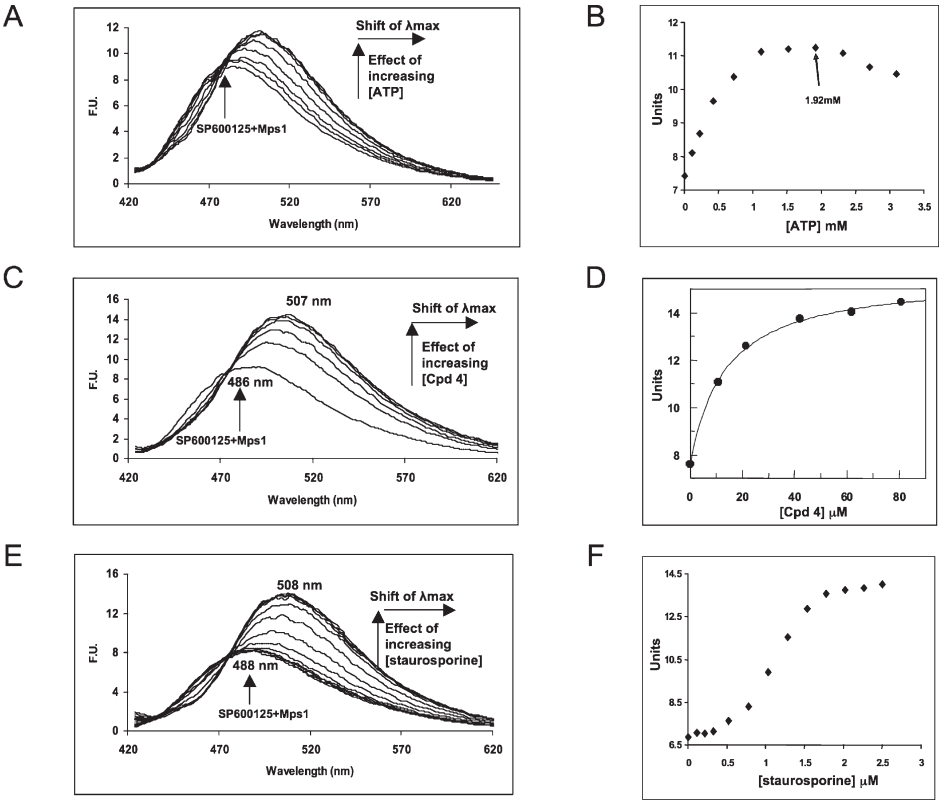

FIGURE 4: Competitive displacement of SP600125 from Mps1 by diverse ligands. (A) Fluorescence emission spectra resulting from addition of aliquots of MgATP to the complex of SP600125 and Mps1, corresponding to spectrum H in Figure 3A in 50 mM Tris buffer, pH 7.4, 150 mM NaCl, and 0.1 mM EGTA at 25 °C, using λ_{exc} 404 nm and [ATP] ranging from 0 to 1.92 mM. (B) Plot of FU (at 508 nm) for the data in (A) corrected for volume change against the concentration of MgATP, recorded as the concentration of ATP added. (C) Fluorescence spectra resulting from addition of Cpd 4 to the mixture of Mps1 and SP600125 corresponding to spectrum H in Figure 3A in 50 mM Tris buffer, pH 7.4, 150 mM NaCl, and 0.1 mM EGTA at 25 °C using λ_{exc} 404 nm. (D) Binding curve for the complex of SP600125 and Mps1 titrated with increasing amounts of Cpd 4 plotting the change (increase) in fluorescence intensity at 508 nm (FU) against the concentration of Cpd 4 after correction for volume changes during the titration. Points are experimental from the data in (C); the line is theoretical for single-site binding with K_d(apparent) of 13.2 ± 1.03 μM and a limiting value of 8.04 ± 0.17 for FU. (E) Fluorescence spectra resulting from addition of staurosporine to the mixture of Mps1 and SP600125 corresponding to spectrum H in Figure 3A in 50 mM Tris buffer, pH 7.4, 150 mM NaCl, and 0.1 mM EGTA at 25 °C using λ_{exc} 404 nm. (F) Plot of FU (at 508 nm) for the data in (E) corrected for volume changes against the concentration of staurosporine.

minimized (Figure 5A). While the adenine and ribose rings are in a relatively stable conformation, the phosphate groups of ATP are highly flexible, exhibiting high average *B* factors of 88.37 Å^2. We do not believe that this is caused by low occupancy of ATP in the Mps1 active site, because increasing the soaking time from 5 to 60 min or 18 h did not lead to any decrease in the observed high temperature factors for the ATP molecule. However, a water molecule, the main-chain NH group of Ser-533, and Gly-534 of the glycine-rich loop all hydrogen bond donate to the α-phosphate oxygens of ATP (Figure 5A), mediating a certain degree of stability at this position despite high overall temperature factors for the ligand, whose flexibility has also been reported when inactive Aurora A kinase is bound to a nucleotide analogue (*42*). In structures of model protein kinases, the phosphate groups of ATP are commonly coordinated by bound divalent metal ion(s) and hydrogen bonds between the conserved catalytic lysine (equivalent to Lys-553 in Mps1), providing additional stability to the triphosphate moiety (*39*, *40*). However, in this Mps1 structure, disruption of ionic pairing between Lys-553 and Glu-571, which likely holds Mps1 in a catalytically inactive conformation (*11*), also prevents hydrogen bonds from forming between Lys-533 and the α- or β-phosphate oxygens. Our Mps1−ATP structure was obtained in the presence of the sodium salt of ATP but in the absence of Mg^{2+} ions during crystal soaking experiments. Subsequently, we have found that the addition of 25 or 50 mM Mg^{2+} ions to Mps1−ATP crystal preparations leads to rapid crystal dissolution, presumably due to changes in the structure of the Mps1−ATP complex. The side chain of the putative Mg^{2+}-chelating residue (Asp-664) points away from the ATP-binding cleft and faces the C-terminal lobe, forming a hydrogen bond with another conserved Mg^{2+}-chelating residue (Asn-652) in the catalytic loop (Figure 5A), suggesting why electron density at the γ-phosphate position is absent. In addition, it is formally possible that the absence of the ATP γ-phosphate is due to enzymatic ATP hydrolysis by Mps1 (although in the absence of Mg^{2+} we believe this is unlikely) or could be caused by degradation of the terminal phosphoester link during X-ray analysis. Regardless of the explanation, the occupancy of the γ-phosphate was set to zero during refinement.

Structure of an Mps1−Staurosporine Complex. We next analyzed the structure of the Mps1 catalytic domain in complex with the research compound staurosporine at a resolution of 2.4 Å (data set 3HMO, Table 2). Staurosporine interacts with nearly all kinases, and this is promoted through a series of highly conserved amino acid interactions in its targets (*43*). Interestingly, the binding of staurosporine (and PEG) to Mps1 (Figure 5B and Supporting Information Figure S1B) occurs in a manner that is very similar to that of the published Mps1−SP600125 inhibitor complex (*11*), and the C_α rmsd between the Mps1−SP600125 and Mps1−staurosporine

Table 2: Data Processing and Refinement Statistics[a]

	data set (PDB ID)		
	WT−ATP (3HMN)	WT−staurosporine (3HMO)	WT−Cpd 4 (3HMP)
data collection			
space group	*I*222	*I*222	*I*222
unit cell parameters (Å)	$a = 70.98$, $b = 104.95$, $c = 111.02$	$a = 70.94$, $b = 103.88$, $c = 111.42$	$a = 71.37$, $b = 103.93$, $c = 111.73$
Matthews coeff ($Å^3 \cdot Da^{1-}$)	2.65	2.63	2.65
solvent content (%)	53.59	53.26	53.69
no. of molecules per ASU[b]	1	1	1
X-ray source	MicroMax007, Rigaku	I03, Diamond	I03, Diamond
wavelength (Å)	1.54	0.92	0.92
resolution (Å)	59.76−2.70 (2.85−2.70)	76.03−2.40 (2.53−2.40)	76.03−2.30 (2.42−2.30)
total reflections	65236	108914	117209
unique reflections	11436	16228	18501
completeness (%)	97.80 (97.00)	98.60 (91.00)	98.40 (90.30)
redundancy	5.7 (5.8)	6.7 (5.0)	6.3 (3.9)
R_{merge}[c] (%)	7.20 (51.90)	10.10 (55.00)	7.30 (39.00)
$\langle I/\sigma(I) \rangle$	21.20 (3.00)	19.10 (5.00)	17.70 (3.00)
refinement			
resolution (Å)	52.47−2.70	76.03−2.40	76.03−2.30
R_{work}[d] (%)	22.10	21.50	21.00
R_{free}[d] (%)	26.50	26.10	24.80
rmsd bond lengths (Å)	0.007	0.007	0.009
rmsd bond angles (deg)	0.973	1.041	1.170
average *B* factors ($Å^2$)/no. of atoms per ASU			
protein non-H atoms	53.60/2083	37.08/2096	37.00/2107
water molecules	48.35/24	40.92/80	42.29/85
ligand non-H atoms	ATP, 80.35/31; PEG, 57.30/16	STU, 49.12/35; PEG, 59.99/16; GOL, 50.82/36; IPA, 45.13/12	Cpd 4, 46.43/16; PEG, 44.68/16; GOL, 45.79/18; IPA, 50.75/12; DEG, 52.55/7
Φ/Ψ angles (%)			
favored regions	96.40	98.00	97.60
additionally allowed regions	3.60	2.00	2.40
disallowed regions	0.00	0.00	0.00

[a]Values in parentheses are for the highest resolution. [b]Asymmetric unit. [c]$R_{merge} = \sum_h \sum_j |I_j(h) - \langle I(h) \rangle| / \sum_h \sum_h I_j(h)$, where $I_j(h)$ is the *j*th measurement of reflection indices *h* and $\langle I(h) \rangle$ is the mean intensity. [d]$R_{work} = \sum_h ||F_o(h)| - |F_c(h)|| / \sum_h |F_o(h)|$; R_{free} was calculated using 5% of data excluded from refinement.

complexes is only 0.556 Å when 256 C_α atoms are aligned. The indole rings of staurosporine are sandwiched by several nonaromatic hydrophobic residues on both sides of the adenine-binding pocket, including Ile-531, Val-539, Ala-551, and Met-602 at the top and Ile-586, Leu-654, and Ile-663 at the bottom, as previously established for SP600125 (*11*). Two conserved hydrogen bonds are formed at the hinge region, one between the N1 of the lactam ring of staurosporine and the Glu-603 main-chain carbonyl oxygen and another between the lactam oxygen O5 at the C8 position and the Gly-605 main-chain NH. There is an additional hydrogen bond formed between the methylamino N4 of staurosporine and the carboxyl group (Oδ1) of Asp-608. This highly conserved interaction helps to explain the relatively high potency of staurosporine for Mps1, in addition to other kinases (*43*). Further inspection of the staurosporine-binding region shows that the inhibitor is stabilized through a C−H···O interaction between the glycosidic oxygen (O4) and the C_α atom of Gly-532 in the glycine loop (Figure 5B). This staurosporine−glycine-rich loop contact mimics the interaction formed between ATP and the glycine-rich loop, and such an interaction has also been observed in several other unrelated kinases in complex with staurosporine, including the tyrosine kinases LCK (*44*) and CSK (*45*) and the Ser/Thr kinases CDK2 (*46*), PDK1 (*43*), and PKA (*47*).

Structure of an Mps1−Compound 4 Complex. To begin to explore structure−activity relationships (SARs) of lead Mps1 inhibitors validated in our biophysical screen, we also determined the structure of Mps1 in complex with the quinazoline Cpd 4 at 2.3 Å resolution (data set 3HMP, Table 2). We initially selected Cpd 4 for structural studies due to its favorable pharmacological profile, although as a low-affinity (micromolar) Mps1 inhibitor it also exhibits the properties of an inhibitor scaffold and can be readily modified for fine-tuning of potency and specificity. As shown in Figure 5C, the aromatic body of Cpd 4 occupies a similar position in the adenine-binding pocket as SP600125. However, Cpd 4 is only sandwiched by four hydrophobic Mps1 residues, namely, Ile-531, Ala-551, Met-602, and Leu-654 (Figure 5C), and only one prototypical hydrogen bond is formed between nitrogen N_{AK} and the Cys-604 main-chain carbonyl oxygen group located in the hinge region. Interestingly, this hinge-region hydrogen bond cannot be observed in any other Mps1 structures, as the peptide bond between Cys-604 and Gly-605 is flipped so that the main-chain NH of Gly-605 can hydrogen bond donate to either ATP or staurosporine (Figure 5A,B). We also identified an unconventional C−H···O bond formed between Cpd 4 and Mps1, with the Cpd 4 aromatic ring C_{AB}−H hydrogen bond donating to the Glu-603 main-chain carbonyl oxygen at the hinge region. A similar, structurally established, C−H···O hydrogen bond has also been observed between a related quinazolin-4-ylthiazol-2-ylamine inhibitor and GSK3 (*48*). Such noncovalent interactions are thought to be somewhat weaker than conventional hydrogen bonds but are clearly important for promoting inhibitor−kinase interactions (*48*, *49*).

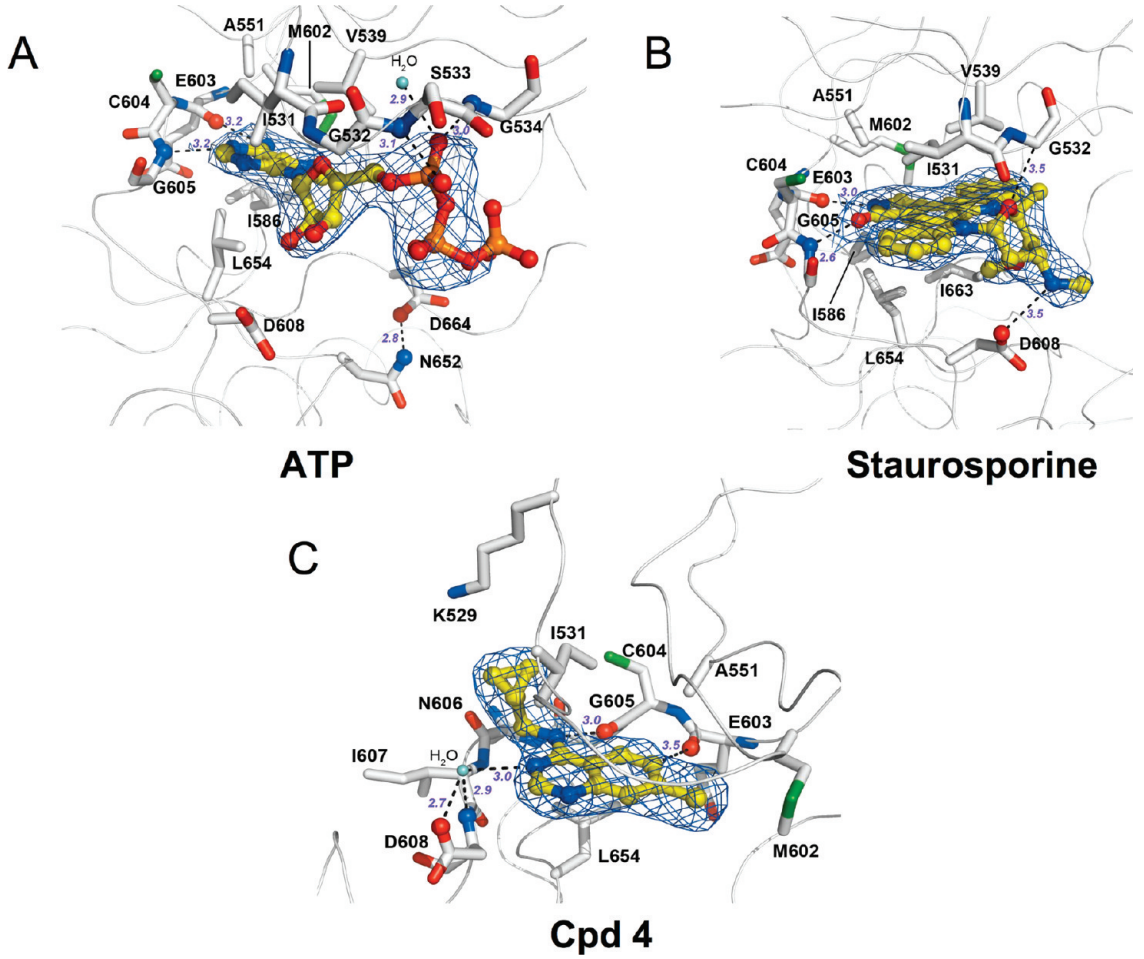

FIGURE 5: 3-D structure of Mps1 complexes. Atom colors for amino acids are blue (nitrogen) and red (oxygen) and for ligands yellow (carbon), blue (nitrogen), red (oxygen), and orange (phosphorus). The residues that interact with ligands are depicted as sticks, and hydrogen bonds are shown as dotted lines, with distances between indicated atoms in angstroms shown in purple. (A) Structural analysis of the Mps1 ATP-binding site. Detailed view of the structure of the Mps1−ATP complex at 2.7 Å resolution, showing ATP bound in the nucleotide-binding site. Note that Asp-608, Asp-664, and Asn-562 do not interact with ATP. A $2F_o - F_c$ map around ATP is shown in blue, contoured at 1.0σ. (B) Structural insights into the staurosporine-binding site. Detailed view of the structure of the Mps1−staurosporine complex at 2.4 Å resolution, showing staurosporine bound in the ATP-binding site. A $2F_o - F_c$ map around staurosporine is shown in blue, contoured at 1.0σ. (C) Interaction of the ATP-competitive quinazoline inhibitor Cpd 4 with Mps1. Detailed view of the structure of the Mps1−Cpd 4 complex at 2.3 Å resolution, showing the inhibitor bound in the ATP-binding site. A water-mediated hydrogen bond network provides Cpd 4 stability, with Cpd 4 N1 and Asp-608 main-chain NH hydrogen bond donating to a water molecule (H_2O, cyan) and a water hydrogen bond to the carboxyl group (Oδ1) of Asp-608. A $2F_o - F_c$ map around Cpd 4 is shown in blue, contoured at 1.0σ.

In addition, a water-mediated hydrogen bond is present between Cpd 4 N1 and the carboxyl group (Oδ1) of Asp-608 of Mps1, which is likely to help to stabilize Cpd 4 in the ATP-binding site. Since Cpd 4 makes fewer van der Waals contacts and fewer conventional hydrogen bonds than other Mps1 inhibitors, such as SP600125 (*11*) and staurosporine (Figure 5B), it is perhaps not surprising that it exhibits a lower inhibitory potency toward Mps1 (Table 1). Superimposition of the Mps1−SP600125 and Mps1−Cpd 4 structures yields an overall rmsd of 0.591 Å for 255 C_α atoms, demonstrating no major changes in conformation between either inhibitor-bound kinase when compared to the apo form of Mps1 (*11*). A molecule of PEG derived from the crystallization medium is also detected in the Mps1−Cpd 4 structure (Supporting Information Figure S1C).

DISCUSSION

The past decade has seen a dramatic growth in the approval rate of protein kinase inhibitors as therapeutic agents (*1*, *2*). This has stimulated the development of an array of analytical techniques to aid in the discovery and development of lead compounds. These include low-to-medium throughput methods, such as radiometric kinase assays (*50*) and fragment-based structural screens of kinases and ligand scaffolds (*3*, *4*, *21*). In addition, high-throughput fluorescence (*32*, *34*), competition (*20*, *51*), and FRET-based proximity reporter assays (*33*) are increasingly sought for the rapid assessment of inhibitor structure−activity relationships, potency, and intrakinome specificity. Most inhibitors described for protein kinases interact with the ATP-binding site present in an active, phosphorylated conformation and have been termed type I inhibitors (*1*). However, an important second class of ligands, the so-called type II inhibitors, is increasingly recognized and sought after due to its potential for increased kinase potency and selectivity (*1*, *52*). These compounds can bind to inactive, often dephosphorylated, forms of kinases and include clinical drugs such as Imantinib (Gleevec), which can target the inactive Abl kinase conformation with some specificity (*1*). The preponderance of inhibitors in the first class no doubt arises from the initial use of enzyme activity assays to screen for them; however, the latter class, which includes allosteric inhibitors, requires some alternative, but direct, biophysical methods for validation.

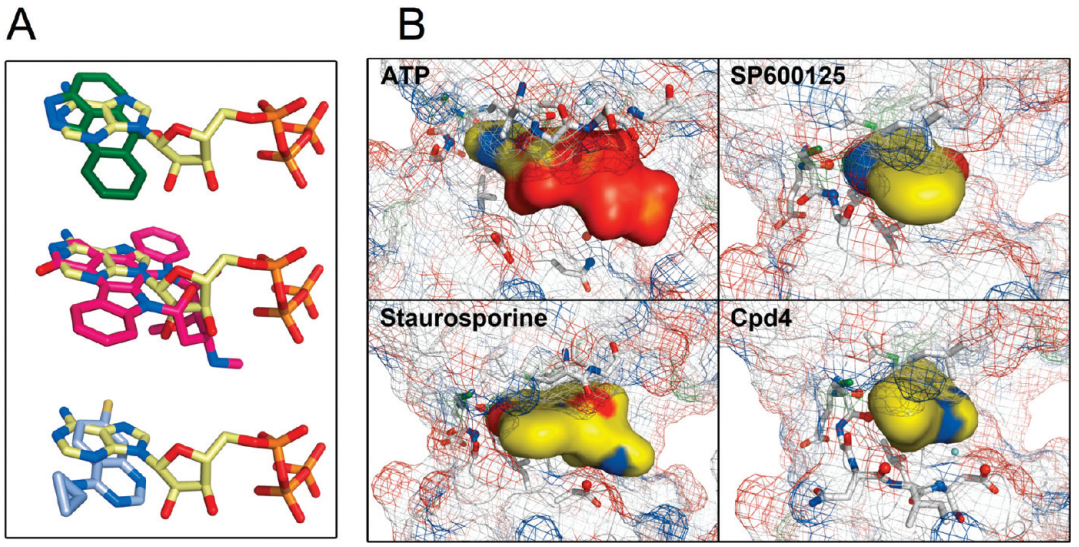

FIGURE 6: Mps1 ligand-binding analysis. (A) Comparison of inhibitor and ATP conformations. The positions of the inhibitors are compared with ATP in the nucleotide-binding site in the Mps1 complexes based on the superposition of the C_α atoms of Mps1. Panels: top, SP600125 (depicted in green and blue) and ATP; middle, staurosporine (depicted in magenta and blue) and ATP; bottom, Cpd 4 (depicted in gray and blue) and ATP. Atom colors for ATP are yellow (carbon), blue (nitrogen), red (oxygen), and orange (phosphorus). (B) Solvent-accessible molecular surfaces of the Mps1−ligand complexes. The solvent-accessible surface of Mps1 is shown as mesh with carbon, nitrogen, and oxygen in white, blue, and red, respectively. The solvent-accessible surfaces of the ligands are represented as solid shapes, with atom colors coded the same as in the legend to Figure 5. The contacting interface areas between Mps1 and ATP, SP600125, staurosporine, and Cpd 4 are 256.4, 206.1, 355.7, and 231.1 Å^2, respectively, calculated using AreaIMol in CCP4i (*36*, *37*).

In this paper, we employ a comparative analysis to prove that the promiscuous kinase inhibitors SP600125, staurosporine, and the quinazoline Cpd 4 bind and inhibit both phosphorylated and experimentally dephosphorylated Mps1 kinases *in vitro* (Figures 1−4). We also demonstrate that the range of Mps1 binding affinities exhibited by these compounds in a biophysical assay compares favorably to IC_{50} values calculated using conventional radiometric analysis (Table 1). In our novel fluorescent assay, excitation of SP600125 at 404 nm leads to emission of the Mps1−SP600125 complex at 486 nm, a Stokes shift of 82 nm. The displacement of SP600125 by ATP-competitive ligands causes the emission wavelength to shift back to that of the free SP600125 (508 nm, a Stokes shift of 104 nm). Fluorescent exploitation of the small, commercially available, SP600125 avoids complex and expensive synthesis steps and should be readily extendable to the 5−10% of the human kinome that are known to interact with this compound (*18*−*20*, *50*). A detailed exemplification of how inherently fluorescent staurosporine and modified analogues can be used in a similar way to that described for SP600125 has recently been described (*32*). However, the excitation wavelength used in this study (296 nm) is close to that of the intrinsic fluorophoric amino acids of proteins, so the discovery of fluorescent ligands such as SP600125, which can be excited in a distinct visible region of the spectrum, is a useful advance. Additional advantages of a displacement assay include the ability to analyze catalytically and conformationally distinct forms of kinases from a range of sources, some of which are unsuitable for radiometric assay or are refractive to X-ray crystallographic analysis due to extensive posttranslational modifications.

Many current techniques used to study inhibition of protein kinases by small molecules, such as radiometric kinase assays, cannot be used to directly provide equilibrium (thermodynamic) values of binding constants for ligand discovery applications, since they generally reflect kinetic parameters (such as IC_{50} or K_i), which are inherently complex. The biophysical studies reported in this study offer a more direct means to determine ligand equilibrium binding constants and might also be modified to carry out detailed kinetic dissections of individual rate processes (e.g., by stopped-flow analysis). Moreover, a SP600125-displacement assay permits the screening of large numbers of compounds in an efficient, quick, and reproducible way and could readily be adopted for high-throughput screening of libraries to identify lead compounds that interact with the ATP-binding site of therapeutically relevant kinases. Examples of such targets are the SP600125-sensitive JNK isoforms (*18*, *20*, *50*), which are catalytically inactive when isolated from bacteria and require activation with an upstream kinase prior to analysis by radiometric techniques. We envisage that the displacement of fluorescent SP600125 from a kinase complex might therefore have wider applications for the generalized discovery of kinase inhibitors.

Mps1−ATP-Binding Site Interactions and Potential for Inhibitor Design. In order to validate the results of our fluorescent assay and effect a molecular analysis of inhibitor binding to Mps1, we determined the crystal structures of the dephosphorylated Mps1 catalytic domain in complex with the physiological ligand ATP and both potent (staurosporine) and weak (Cpd 4) inhibitors of Mps1 enzyme activity. Our structures indicate that staurosporine and Cpd 4 can displace SP600125 from Mps1 because they both bind directly to similar loci in the Mps1 ATP-binding site, whose structurally inactive conformation is permissive for interaction with all of these compounds (Supporting Information Figure S1A−C). Superimposition of the Mps1−ATP and Mps1−inhibitor complexes from the X-ray structures highlights very similar molecular modes of binding to Mps1 (Figure 6A). The functional indazole ring system of SP600125, the lactam ring of staurosporine, and the quinazoline ring structure of Cpd 4 occupy similar positions in the adenine-binding pocket, forming hydrogen bonds to the kinase hinge region. All of the heterocyclic rings of the inhibitors also make hydrophobic interactions with residues in the nucleotide-binding pocket, in a manner similar to that of the adenine ring of ATP

(Figure 5A). This structural analysis also supports our biochemical and biophysical data, which concur that staurosporine is the most potent Mps1 inhibitor among our panel of compounds (Table 1). In further agreement with these findings, we demonstrate in Figure 6B that staurosporine also exhibits the greatest area of molecular contact with Mps1 (355.7 Å^2), when compared alongside ATP (256.4 Å^2), SP600125 (206.1 Å^2), or Cpd 4 (231.1 Å^2).

Staurosporine is perhaps the most intensively studied and nonspecific kinase inhibitor described to date, with reported affinities for kinases ranging over some 6 orders of magnitude (*51*). A detailed knowledge of the interaction mode with multiple protein kinases has prompted chemical modification in an attempt to produce more specific and potent kinase inhibitors. Staurosporine derivatives such as PKC-412 and UCN-01, while also exhibiting a high degree of *in vitro* promiscuity (*43*, *51*, *53*), have demonstrated promise in preclincial studies and received approval for clinical trials as cancer therapies, yet ultimately have failed to reach the market. However, despite staurosporine's lack of success as a marketed drug, useful information can still be derived from its specific mode of binding for potential use with other chemical scaffolds. We report that the sugar methylamino group of staurosporine forms a conserved hydrogen bond with Asp-608 in the Mps1 glycine-rich loop (Figure 5B). In contrast, a hydrogen bond that is commonly found in kinase complexes with staurosporine is not formed between the methylamino N4 of the compound and the main-chain carbonyl oxygen of Mps1. Instead, the carbonyl oxygen is positioned near to the methoxyl O6, which to our knowledge has not been observed with other kinases. Therefore, we speculate that a basic substitution at O6 of staurosporine might encourage the formation of a hydrogen bond with this available carbonyl oxygen, enhancing the potency of a staurosporine homologue toward Mps1 and potentially desensitizing it toward other kinases.

Cpd 4 is a quinazoline scaffold, which has already been shown to be an amenable chemical template for successful drugs including the EGFR kinase inhibitors Gefitinib (Iressa), Erlotinib (Tarceva), and Lapatinib (Tykerb, refs (*54*−*56*)). In the current study, we show that Cpd 4 interacts with the ATP-binding site of Mps1 in a similar manner when compared to either staurosporine or SP600125 (Figure 6). Cpd 4 demonstrates a relatively low potency for Mps1 and serves as a prototypic fragment for future structure-based medicinal chemistry efforts. In this regard, several quinazoline compounds exhibit significantly lower IC_{50} values for Mps1 inhibition *in vitro*, including the closely related inhibitor Cpd 1 (Figure 1B), which we are currently assessing as a lead Mps1 inhibitor candidate. By combining the novel scaffold of Cpd 4 and its relatives with the potent Mps1 inhibitory effects of staurosporine, our Mps1 crystal structures can provide useful insights for the design of improved Mps1 inhibitors. For example, a methyl or similar hydrophobic substitution of the chloride atom of Cpds 1 or 4 might provide additional van der Waals contacts with the adjacent gatekeeper residue Met-602 of Mps1 (Figure 5C). The casual importance of the region containing this Met residue for inhibition of human Mps1 has previously been established for SP600125 (*11*, *19*). In addition, the C_{AB} atom of Cpd 4 might be substituted for a nitrogen atom to attempt to mimic the interaction between the hinge region and the lactam ring observed in the Mps1−staurosporine structure (Figure 5B). As shown in Figure 5C, Ile-607 is in close proximity to the cyclopropanyl ring of Cpd 4, and this hydrophobic side chain is not highly conserved between kinases. A more bulky hydrophobic group attached to, or substituted for, this group might provide extra hydrophobic contacts with the side chain of Ile-607, thus increasing the potency and selectivity of such a compound. Similarly, Lys-529, a basic residue located outside the ATP-binding pocket, is also positioned close to the cyclopropanyl ring (Figure 5C), and the effects of introducing a polar group at this position on inhibitor potency toward Mps1 are worthy of investigation.

We previously reported for both apo-Mps1 and an Mps1−SP600125 complex the existence of a secondary binding pocket, which is created by the disruption of the conserved Lys-Glu catalytic ion pair flanking the nucleotide-binding site in Mps1 (*11*). This region is not utilized by the inhibitor or ATP and represents a potential allosteric type of drug-binding site. We demonstrate that SP600125 binds with similar affinity to both dephosphorylated and phosphorylated (active) Mps1 (Figure 3) and that ATP, staurosporine (Figure 5B), and Cpd 4 (Figure 5C) all bind in an analogous manner to Mps1, adjacent to a Lys-553-chelated PEG molecule from the crystallization medium (Supporting Information Figure S1A−C). These findings suggest that all of the compounds described in this study could be chemically modified to encourage an extended inhibitor to simultaneously occupy both the ATP- and PEG-binding pockets of dephosphorylated Mps1, and we are currently working toward creating such molecules.

In conclusion, the *in silico*, biochemical, biophysical, and structural information presented in this paper will help to motivate future Mps1 drug design studies, whose goal is the development of potent and selective Mps1 inhibitors for testing and validation in cellular and preclinical cancer models. Our finding that the clinically approved and well-studied quinazoline class of compounds also represents a novel source of Mps1 inhibitors suggests one logical direction for such efforts in the near future.

ACKNOWLEDGMENT

We thank Dr. John Rafferty, Dr. David Robinson, and Dr. Michael Trikic for comments on the manuscript.

SUPPORTING INFORMATION AVAILABLE

One additional figure detailing the structural conformation of the PEG-bound Mps1 kinase domain (residues 510−809) in complex with ATP, staurosporine, or Cpd 4 and two additional tables, detailing both desirable and undesirable features that were enforced to generate our *in silico* inhibitor library. This material is available free of charge via the Internet at http://pubs.acs.org.

REFERENCES

1. Zhang, J., Yang, P. L., and Gray, N. S. (2009) Targeting cancer with small molecule kinase inhibitors. *Nat. Rev. Cancer 9*, 28–39.
2. Cohen, P. (2009) Targeting protein kinases for the development of anti-inflammatory drugs. *Curr. Opin. Cell Biol. 21*, 317–324.
3. Cherry, M., Reader, J., and Williams, D. (2006) Finding protein kinase hits using structural information. *Prog. Med. Chem. 44*, 1–63.
4. Cherry, M., and Williams, D. H. (2004) Recent kinase and kinase inhibitor X-ray structures: mechanisms of inhibition and selectivity insights. *Curr. Med. Chem. 11*, 663–673.
5. Fisk, H. A., Mattison, C. P., and Winey, M. (2003) Human Mps1 protein kinase is required for centrosome duplication and normal mitotic progression. *Proc. Natl. Acad. Sci. U.S.A. 100*, 14875–14880.
6. Jelluma, N., Brenkman, A. B., van den Broek, N. J., Cruijsen, C. W., van Osch, M. H., Lens, S. M., Medema, R. H., and Kops, G. J. (2008) Mps1 phosphorylates Borealin to control Aurora B activity and chromosome alignment. *Cell 132*, 233–246.

7. Kang, J., Chen, Y., Zhao, Y., and Yu, H. (2007) Autophosphorylation-dependent activation of human Mps1 is required for the spindle checkpoint. *Proc. Natl. Acad. Sci. U.S.A. 104*, 20232–20237.
8. Mattison, C. P., Old, W. M., Steiner, E., Huneycutt, B. J., Resing, K. A., Ahn, N. G., and Winey, M. (2007) Mps1 activation loop autophosphorylation enhances kinase activity. *J. Biol. Chem. 282*, 30553–30561.
9. Tyler, R. K., Chu, M. L., Johnson, H., McKenzie, E. A., Gaskell, S. J., and Eyers, P. A. (2009) Phosphoregulation of human Mps1 kinase. *Biochem. J. 417*, 173–181.
10. Jelluma, N., Brenkman, A. B., McLeod, I., Yates, J. R., III, Cleveland, D. W., Medema, R. H., and Kops, G. J. (2008) Chromosomal instability by inefficient Mps1 auto-activation due to a weakened mitotic checkpoint and lagging chromosomes. *PLoS One 3*, e2415.
11. Chu, M. L., Chavas, L. M., Douglas, K. T., Eyers, P. A., and Tabernero, L. (2008) Crystal structure of the catalytic domain of the mitotic checkpoint kinase Mps1 in complex with SP600125. *J. Biol. Chem. 283*, 21495–21500.
12. Wang, W., Yang, Y., Gao, Y., Xu, Q., Wang, F., Zhu, S., Old, W., Resing, K., Ahn, N., Lei, M., and Liu, X. (2008) Structural and mechanistic insights into Mps1 kinase activation. *J. Cell Mol. Med. 13*, 1679–1694.
13. Kops, G. J., Weaver, B. A., and Cleveland, D. W. (2005) On the road to cancer: aneuploidy and the mitotic checkpoint. *Nat. Rev. Cancer 5*, 773–785.
14. Iwase, T., Tanaka, M., Suzuki, M., Naito, Y., Sugimura, H., and Kino, I. (1993) Identification of protein-tyrosine kinase genes preferentially expressed in embryo stomach and gastric cancer. *Biochem. Biophys. Res. Commun. 194*, 698–705.
15. Janssen, A., Kops, G. J., and Medema, R. H. (2009) Elevating the frequency of chromosome mis-segregation as a strategy to kill tumor cells. *Proc. Natl. Acad. Sci. U.S.A. 106*, 19108–19113.
16. Swanton, C., Marani, M., Pardo, O., Warne, P. H., Kelly, G., Sahai, E., Elustondo, F., Chang, J., Temple, J., Ahmed, A. A., Brenton, J. D., Downward, J., and Nicke, B. (2007) Regulators of mitotic arrest and ceramide metabolism are determinants of sensitivity to paclitaxel and other chemotherapeutic drugs. *Cancer Cell 11*, 498–512.
17. Dorer, R. K., Zhong, S., Tallarico, J. A., Wong, W. H., Mitchison, T. J., and Murray, A. W. (2005) A small-molecule inhibitor of Mps1 blocks the spindle-checkpoint response to a lack of tension on mitotic chromosomes. *Curr. Biol. 15*, 1070–1076.
18. Bennett, B. L., Sasaki, D. T., Murray, B. W., O'Leary, E. C., Sakata, S. T., Xu, W., Leisten, J. C., Motiwala, A., Pierce, S., Satoh, Y., Bhagwat, S. S., Manning, A. M., and Anderson, D. W. (2001) SP600125, an anthrapyrazolone inhibitor of Jun N-terminal kinase. *Proc. Natl. Acad. Sci. U.S.A. 98*, 13681–13686.
19. Schmidt, M., Budirahardja, Y., Klompmaker, R., and Medema, R. H. (2005) Ablation of the spindle assembly checkpoint by a compound targeting Mps1. *EMBO Rep. 6*, 866–872.
20. Fabian, M. A., Biggs, W. H., III, Treiber, D. K., Atteridge, C. E., Azimioara, M. D., Benedetti, M. G., Carter, T. A., Ciceri, P., Edeen, P. T., Floyd, M., Ford, J. M., Galvin, M., Gerlach, J. L., Grotzfeld, R. M., Herrgard, S., Insko, D. E., Insko, M. A., Lai, A. G., Lelias, J. M., Mehta, S. A., Milanov, Z. V., Velasco, A. M., Wodicka, L. M., Patel, H. K., Zarrinkar, P. P., and Lockhart, D. J. (2005) A small molecule-kinase interaction map for clinical kinase inhibitors. *Nat. Biotechnol. 23*, 329–336.
21. Matthews, T. P., Klair, S., Burns, S., Boxall, K., Cherry, M., Fisher, M., Westwood, I. M., Walton., M. I., McHardy, T., Cheung, K.-M. J., Van Mortfort, R., Williams, D. H., Aherne, G. W., Garrett, M. D., Reader, J., and Collins, I. (2009) Identification of inhibitors of checkpoint kinase 1 through template screening. *J. Med. Chem. 52*, 4810–4819.
22. Leslie, A. G. W. (1992) in *Joint CCP4 and ESF-EACBM Newsletter 26*.
23. Evans, P. R. (1997) in *Joint CCP4 and ESF-EACBM Newsletter 33*.
24. Murshudov, G. N., Vagin, A. A., and Dodson, E. J. (1997) Refinement of macromolecular structures by the maximum-likelihood method. *Acta Crystallogr., Sect. D: Biol. Crystallogr. 53*, 240–255.
25. Adams, P. D., Grosse-Kunstleve, R. W., Hung, L. W., Ioerger, T. R., McCoy, A. J., Moriarty, N. W., Read, R. J., Sacchettini, J. C., Sauter, N. K., and Terwilliger, T. C. (2002) PHENIX: building new software for automated crystallographic structure determination. *Acta Crystallogr., Sect. D: Biol. Crystallogr. 58*, 1948–1954.
26. Emsley, P., and Cowtan, K. (2004) Coot: model-building tools for molecular graphics. *Acta Crystallogr., Sect. D: Biol. Crystallogr. 60*, 2126–2132.
27. Davis, I. W., Leaver-Fay, A., Chen, V. B., Block, J. N., Kapral, G. J., Wang, X., Murray, L. W., Arendall, W. B., III, Snoeyink, J., Richardson, J. S., and Richardson, D. C. (2007) MolProbity: all-atom contacts and structure validation for proteins and nucleic acids. *Nucleic Acids Res. 35*, W375–W383.
28. DeLano, W. L. (2005) The case for open-source software in drug discovery. *Drug Discov. Today 10*, 213–217.
29. Wang, Z. X. (1995) An exact mathematical expression for describing competitive binding of two different ligands to a protein molecule. *FEBS Lett. 360*, 111–114.
30. Heron, N. M., Anderson, M., Blowers, D. P., Breed, J., Eden, J. M., Green, S., Hill, G. B., Johnson, T., Jung, F. H., McMiken, H. H., Mortlock, A. A., Pannifer, A. D., Pauptit, R. A., Pink, J., Roberts, N. J., and Rowsell, S. (2006) SAR and inhibitor complex structure determination of a novel class of potent and specific Aurora kinase inhibitors. *Bioorg. Med. Chem. Lett. 16*, 1320–1323.
31. Girdler, F., Gascoigne, K. E., Eyers, P. A., Hartmuth, S., Crafter, C., Foote, K. M., Keen, N. J., and Taylor, S. S. (2006) Validating Aurora B as an anti-cancer drug target. *J. Cell Sci. 119*, 3664–3675.
32. Iyer, G. H., Taslimi, P., and Pazhanisamy, S. (2008) Staurosporine-based binding assay for testing the affinity of compounds to protein kinases. *Anal. Biochem. 373*, 197–206.
33. Lebakken, C. S., Hee, C. K., and Vogel, K. W. (2007) A fluorescence lifetime based binding assay to characterize kinase inhibitors. *J. Biomol. Screening 12*, 828–841.
34. Kawaguchi, M., Terai, T., Utata, R., Kato, M., Tsuganezawa, K., Tanaka, A., Kojima, H., Okabe, T., and Nagano, T. (2008) Development of a novel fluorescent probe for fluorescence correlation spectroscopic detection of kinase inhibitors. *Bioorg. Med. Chem. Lett. 18*, 3752–3755.
35. Johnson, H., Eyers, C. E., Eyers, P. A., Beynon, R. J., Gaskell, S. J. (2009) Rigorous determination of the stoichiometry of protein phosphorylation using mass spectrometry. *J. Am. Soc. Mass Spectrom. 20*, 2211−2220.
36. Krissinel, E., and Henrick, K. (2004) Secondary-structure matching (SSM), a new tool for fast protein structure alignment in three dimensions. *Acta Crystallogr., Sect. D: Biol. Crystallogr. 60*, 2256–2268.
37. Collaborative Computational Project, Number 4 (1994) The CCP4 suite: programs for protein crystallography, Acta Crystallogr., Sect. D: Biol. Crystallogr. *50*, 760−763.
38. De Bondt, H. L., Rosenblatt, J., Jancarik, J., Jones, H. D., Morgan, D. O., and Kim, S. H. (1993) Crystal structure of cyclin-dependent kinase 2. *Nature 363*, 595–602.
39. Owen, D. J., Noble, M. E., Garman, E. F., Papageorgiou, A. C., and Johnson, L. N. (1995) Two structures of the catalytic domain of phosphorylase kinase: an active protein kinase complexed with substrate analogue and product. *Structure 3*, 467–482.
40. Schulze-Gahmen, U., De Bondt, H. L., and Kim, S. H. (1996) High-resolution crystal structures of human cyclin-dependent kinase 2 with and without ATP: bound waters and natural ligand as guides for inhibitor design. *J. Med. Chem. 39*, 4540–4546.
41. Zheng, J., Knighton, D. R., ten Eyck, L. F., Karlsson, R., Xuong, N., Taylor, S. S., and Sowadski, J. M. (1993) Crystal structure of the catalytic subunit of cAMP-dependent protein kinase complexed with MgATP and peptide inhibitor. *Biochemistry 32*, 2154–2161.
42. Bayliss, R., Sardon, T., Vernos, I., and Conti, E. (2003) Structural basis of Aurora-A activation by TPX2 at the mitotic spindle. *Mol. Cell 12*, 851–862.
43. Komander, D., Kular, G. S., Bain, J., Elliott, M., Alessi, D. R., and Van Aalten, D. M. (2003) Structural basis for UCN-01 (7-hydroxy-staurosporine) specificity and PDK1 (3-phosphoinositide-dependent protein kinase-1) inhibition. *Biochem. J. 375*, 255–262.
44. Zhu, X., Kim, J. L., Newcomb, J. R., Rose, P. E., Stover, D. R., Toledo, L. M., Zhao, H., and Morgenstern, K. A. (1999) Structural analysis of the lymphocyte-specific kinase Lck in complex with non-selective and Src family selective kinase inhibitors. *Structure 7*, 651–661.
45. Lamers, M. B., Antson, A. A., Hubbard, R. E., Scott, R. K., and Williams, D. H. (1999) Structure of the protein tyrosine kinase domain of C-terminal Src kinase (CSK) in complex with staurosporine. *J. Mol. Biol. 285*, 713–725.
46. Lawrie, A. M., Noble, M. E., Tunnah, P., Brown, N. R., Johnson, L. N., and Endicott, J. A. (1997) Protein kinase inhibition by staurosporine revealed in details of the molecular interaction with CDK2. *Nat. Struct. Biol. 4*, 796–801.
47. Prade, L., Engh, R. A., Girod, A., Kinzel, V., Huber, R., and Bossemeyer, D. (1997) Staurosporine-induced conformational changes of cAMP-dependent protein kinase catalytic subunit explain inhibitory potential. *Structure 5*, 1627–1637.
48. Pierce, A. C., ter, H. E., Binch, H. M., Kay, D. P., Patel, S. R., and Li, P. (2005) CH···O and CH···N hydrogen bonds in ligand design: a

novel quinazolin-4-ylthiazol-2-ylamine protein kinase inhibitor. *J. Med. Chem. 48*, 1278–1281.
49. Pierce, A. C., Sandretto, K. L., and Bemis, G. W. (2002) Kinase inhibitors and the case for CH···O hydrogen bonds in protein-ligand binding. *Proteins 49*, 567–576.
50. Bain, J., McLauchlan, H., Elliott, M., and Cohen, P. (2003) The specificities of protein kinase inhibitors: an update. *Biochem. J. 371*, 199–204.
51. Karaman, M. W., Herrgard, S., Treiber, D. K., Gallant, P., Atteridge, C. E., Campbell, B. T., Chan, K. W., Ciceri, P., Davis, M. I., Edeen, P. T., Faraoni, R., Floyd, M., Hunt, J. P., Lockhart, D. J., Milanov, Z. V., Morrison, M. J., Pallares, G., Patel, H. K., Pritchard, S., Wodicka, L. M., and Zarrinkar, P. P. (2008) A quantitative analysis of kinase inhibitor selectivity. *Nat. Biotechnol. 26*, 127–132.
52. Bogoyevitch, M. A., and Fairlie, D. P. (2007) A new paradigm for protein kinase inhibition: blocking phosphorylation without directly targeting ATP binding. *Drug Discov. Today 12*, 622–633.
53. Gescher, A. (2000) Staurosporine analogues—pharmacological toys or useful antitumour agents? *Crit Rev. Oncol. Hematol. 34*, 127–135.
54. Barker, A. J., Gibson, K. H., Grundy, W., Godfrey, A. A., Barlow, J. J., Healy, M. P., Woodburn, J. R., Ashton, S. E., Curry, B. J., Scarlett, L., Henthorn, L., and Richards, L. (2001) Studies leading to the identification of ZD1839 (Iressa): an orally active, selective epidermal growth factor receptor tyrosine kinase inhibitor targeted to the treatment of cancer. *Bioorg. Med. Chem. Lett. 11*, 1911–1914.
55. Bulgaru, A. M., Mani, S., Goel, S., and Perez-Soler, R. (2003) Erlotinib (Tarceva): a promising drug targeting epidermal growth factor receptor tyrosine kinase. *Exp. Rev. Anticancer Ther. 3*, 269–279.
56. Rusnak, D. W., Affleck, K., Cockerill, S. G., Stubberfield, C., Harris, R., Page, M., Smith, K. J., Guntrip, S. B., Carter, M. C., Shaw, R. J., Jowett, A., Stables, J., Topley, P., Wood, E. R., Brignola, P. S., Kadwell, S. H., Reep, B. R., Mullin, R. J., Alligood, K. J., Keith, B. R., Crosby, R. M., Murray, D. M., Knight, W. B., Gilmer, T. M., and Lackey, K. (2001) The characterization of novel, dual ErbB-2/EGFR, tyrosine kinase inhibitors: potential therapy for cancer. *Cancer Res. 61*, 7196–7203.